Published in final edited form as:
Circ Res. 2011 December 9; 109(12): 1342–1353. doi:10.1161/CIRCRESAHA.111.255075.

Nuclear Plakoglobin Is Essential for Differentiation of Cardiac Progenitor Cells to Adipocytes in Arrhythmogenic Right Ventricular Cardiomyopathy

Raffaella Lombardi, MD, PhD, **Maria da Graca Cabreira-Hansen, PhD**, **Achim Bell, PhD**, **Richard R. Fromm**, **James T. Willerson, MD**, and **A.J. Marian, MD**
Center for Cardiovascular Genetics, Institute of Molecular Medicine and Department of Medicine, University of Texas Health Sciences Center at Houston, and Texas Heart Institute at St. Luke's Episcopal Hospital, Houston, Texas.

Abstract

Rationale—Arrhythmogenic right ventricular cardiomyopathy (ARVC) is a disease of desmosome proteins characterized by fibroadipogenesis in the myocardium. We have implicated signaling properties of junction protein plakoglobin (PG) in the pathogenesis of ARVC.

Objective—To delineate the pathogenic role of PG in adipogenesis in ARVC.

Methods and Results—We generated mice overexpressing PG, either a wildtype (PG^{WT}) or a truncated (PG^{TR}), known to cause ARVC, in the heart; and PG null ($PG^{-/-}$) embryos. PG^{WT} and PG^{TR} mice exhibited fibro-adiposis, cardiac dysfunction, and premature death. Subcellular protein fractionation and immunofluorescence showed nuclear localization of PG^{WT} and PG^{TR} and reduced membrane localization of PG^{TR}. Coimmunoprecipitation showed reduced binding of PG^{TR} but not PG^{WT} to desmosome proteins DSP and DSG2. Transgene PG^{WT} and PG^{TR} were expressed in c-Kit^{+}:$Sca1^{+}$ cardiac progenitor cells (CPCs) isolated from the hearts of PG^{WT} and PG^{TR} by fluorescence activated cell sorting. CPCs isolated from the transgenic hearts showed enhanced adipogenesis, increased levels of adipogenic factors KLF15, C/EBP-α and noncanonical Wnt5b, and reduced level of CTGF, an inhibitor of adipogenesis. Treatment with BIO activated the canonical Wnt signaling, reversed the proadipogenic transcriptional switch and prevented adipogenesis in a dose-dependent manner. Moreover, c-Kit^{+} CPCs, isolated from $PG^{-/-}$ embryos, were resistant to adipogenesis, expressed high mRNA levels of CTGF and other canonical Wnt signaling targets.

Conclusions—Nuclear PG provokes adipogenesis in c-Kit^{+} CPCs by repressing the canonical Wnt signaling and inducing a proadipogenic gene expression. The findings suggest that adipocytes in ARVC, at least in part, originate from c-Kit^{+} CPCs.

Keywords

cardiomyopathy; genetics; adipogenesis; Wnt signaling; progenitor cells

Arrhythmogenic right ventricular cardiomyopathy (ARVC) is an enigmatic disease characterized by fibroadipocytic replacement of cardiac myocytes, predominantly in the

Correspondence to A.J. Marian, MD, 6770 Bertner Street, Suite C900A, Houston, TX 77030. Ali.J.Marian@uth.tmc.edu.
Achim Bell is currently affiliated with University of Mississippi Medical Center, Jackson.

Disclosures
None.

right ventricle.[1–3] The phenotype is unique, progressive, and without an effective therapy. Progressive fibroadipogenesis, myocytes drop-out, and molecular remodeling lead to cardiac arrhythmias, ventricular dysfunction, and premature death.[1–3] ARVC is an important cause of sudden cardiac death in the young.[1]

Molecular pathogenesis of ARVC has remained elusive since its modern description more than 3 decades ago.[4] Molecular genetic studies have partially elucidated genetic causes of ARVC and provided insights into its pathogenesis. Mutations in genes encoding junction protein plakoglobin (PG), plakophillin 2 (PKP2), desmoplakin (DSP), desmoglein 2 (DSG2), and desmocollin 2 (DSC2) are collectively responsible for about 50% of ARVC cases.[5–11] Mutations in non-desmosome proteins *TGFB3* and *TMEM43* also have been reported in families with ARVC.[12,13] ARVC, at least in a subset, is a disease of desmosome proteins.

To delineate the molecular pathogenesis of ARVC, we have focused on the signaling functions of PG, aka γ-catenin.[14,15] PG, a member of the Armadillo arm proteins, has structural and functional similarities to β-catenin, the signal transducer of the canonical Wnt signaling through Tcf7l2/Lef1 transcription factors.[16] PG is implicated in competitive interactions with β-catenin in regulating various pathways, such as binding to Tcf7l2, ubiquitination, incorporation into adherens junctions, and even desmosome assembly. [17,18] The precise nature of these interactions is not adequately defined and appears to be context dependent. PG and β-catenin differ in their propensities binding to Tcf7l2.[17,18] Accordingly, β-catenin exhibits a strong transcriptional activity through Tcf7l2 and provokes gene expression. In contrast, PG exhibits weak Tcf7l2-mediated transcriptional activity. Consequently, the net effect of binding of PG to Tcf7l2 is suppression of the canonical Wnt signaling. Canonical Wnt signaling not only regulates cell proliferation but also is a major transcriptional switch regulator of myogenesis versus adipogenesis.[19] Thus, PG is a structural protein constituent of desmosomes as well as a signaling molecule that regulates the canonical Wnt signaling.

We have implicated signaling functions of PG in the pathogenesis of ARVC.[14] Accordingly, impaired desmosome assembly in ARVC leads to nuclear localization of PG, repression of the canonical Wnt signaling and enhanced adipogenesis.[14] Absence of PG at the cell junction has been advocated as a diagnostic marker for ARVC in humans.[20] Through a series of genetic-fate mapping experiments, we have identified the second heart field cardiac progenitor cells (CPCs) as a cell source for excess adipocytes in ARVC. However, the direct role of PG in ARVC remains untested. We performed a series of experiments analogous to gain- and loss-of-function studies by overexpressing either a wildtype PG (PG^{WT}) or a truncated PG (PG^{TR}), known to cause ARVC in humans,[11] in cardiac myocyte-lineage and genetically deleting PG in embryos ($PG^{-/-}$). We isolated c-Kit^{+}:$Sca1^{+}$ CPCs from the hearts of PG transgenic mice and $PG^{-/-}$ embryos, determined differentiation of these CPCs to adipocytes, and delineated the responsible molecular mechanisms.

Methods

The investigation conforms to the Guide for the Care and Use of Laboratory Animals published by the US National Institutes of Health and was approved by the Institutional Animal Care and Use Committee.

Genetically Modified Mice

PG^{WT} and PG^{TR} (FVB background) were generated per conventional methods. To distinguish transgene PG^{WT} from the endogenous PG (PG^{Endo}), 3 sequential Flag epitopes were positioned at the N-terminal domain of PG. To generate the deletion construct (PG^{TR}),

we induced a 2-bases deletion ($PG^{23654del2}$) by site-directed mutagenesis. The deletion mutation introduces 11 new amino acids and leads to premature termination of the protein in humans[11] (Figure 1A). The new sequence was used to synthesize a peptide and generate a PG^{TR}-specific antibody. Specificity of the antibody was detected by immunoblotting as shown in Online Figure I (see Online Supplement available at http://circres.ahajournals.org).

Because of embryonic lethality of $PG^{-/-}$,[21] heterozygous ($PG^{\pm}$) mice (C57BL/6 background) were maintained and crossed to generate $PG^{-/-}$ embryo for isolation of CPCs. We also crossed PG^{TR} and $PG^{\pm}$ mice to generate bigenic mice expressing PG^{TR} in the background of deficiency of PG^{Endo}.

Survival, Gross Cardiac Morphology, and Histology

Survival rates were compared by Kaplan–Meier survival analysis. Ventricular/body weight ratios were measured in age- and sex-matched mice. Echocardiography was performed as described.[15,22] Electrocardiograms were also recorded. Myocardial histology was examined by H&E and Masson Trichrome staining of thin sections. Adipocytes were detected by Oil Red O (ORO) staining and C/EBP-α immunostaining, as published.[15,22]

Immunoblotting

Aliquots of ventricular tissue (50 mg) were homogenized using a Covaris Sonicator in RIPA buffer containing complete protease inhibitors. Protein concentration was determined by Lowry assay. Aliquots of 20-μg protein extracts were electrophoresed for immunoblotting. Antibodies were anti-Flag, mutant PG-specific, and pan PG to detect PG^{WT}, PG^{TR}, and transgene plus PG^{Endo} on the same blot, respectively.

Immunofluorescence

Thin myocardial sections and isolated cells were immunostained using anti-pan PG, Flag, PG^{TR}, C/EBP-α, and c-Kit antibodies, as described.[14,15] The samples were mounted in DAPI-containing Hard SetTM mounting medium.

Cell Protein Subfractionation

Nuclear, cytosolic, and membrane proteins were extracted, as published. [15,22] Aliquots of 30 μg of proteins were used for immunoblotting and probed with pan-PG, PG^{TR}, and Flag (PG^{WT}) antibodies. Membranes were stripped in Restore Plus stripping buffer and were reprobed with antibodies against α-tubulin, Lamin A, and C×43 to test purity of the separation.

Coimmunoprecipitation (Co-IP)

Co-IP was performed as described.[15,22] Anti-DSP1/2, DSC2, and DSG2 antibodies were added to 500 μg aliquot of total protein extracts followed by precipitating the antibody-protein complexes by Protein A/G PLUS-Agarose beads and centrifugation. The final pellets were resuspended in a loading buffer and used for immunoblotting.

Isolation and Culture of CPCs from Adult Mouse Hearts

Hearts from 2- to 3-month-old mice were depleted from mature myocytes through digestion with 0.1% type 2 collagenase in α-MEM medium. Cell suspensions were sequentially passed through 70-μm, 40-μm, and 35-μm mesh strainers to eliminate residual mature myocytes and cell aggregates. The cell pellets were washed in MACS Buffer, and incubated with monoclonal antibodies to Sca1 and c-Kit.

C-Kit$^+$, Sca1$^+$, and c-Kit$^+$:Sca1$^+$ cells were sorted using a FACS-Aria flow cytometer. The c-Kit$^+$ cells were negative for markers of the myeloid, lymphoid, and erythroid lineages. After sorting, cells were seeded into 0.1% gelatin-coated plates and supplemented with 10% embryonic stem cell certified FBS, 10 ng/mL mouse basic fibroblast growth factor (bFGF), 1000 U/mL of mouse leukemia inhibitory factor (mLIF), and 1% antibiotic–antimycotic. All the experiments were conducted on cells yielded from the third to fifth passage.

Isolation and Culture of PG$^{+/+}$ and PG$^{-/-}$ CPCs

PG$^{-/-}$ embryos were harvested at E11, separated from placenta and membranes under a dissecting microscope, and genotyped by direct PCR. PG$^{+/+}$ and PG$^{-/-}$ null embryos were used to isolate CPCs.

To isolate CPCs, we incubated embryonal cells with mouse lineage antibodies cocktail and antibodies against Flk1, Sca1, and c-Kit. The FACS-Aria flow cytometer was used to identify and sort c-Kit$^+$, Sca1$^+$, and c-Kit$^+$:Sca1$^+$ cells from the population negative for markers of the myeloid, lymphoid, and erythroid lineages (CD34, CD45, CD20, CD45RO, CD8, and TER-119) and endothelial marker Flk1.

RT-PCR

Total RNA was isolated from CPCs using Qiagen RNeasy Mini Kit. To eliminate genomic DNA, the extracts were treated with DNase 1 sequentially with 2 different DNAse reagents. Aliquots of 2 μg of total RNA were reverse transcribed using SuperScript III First-Strand Synthesis System and oligo dT primers. The RT products were amplified by PCR using primers designed to specifically amplify PG^{Endo}, PG^{WT}, PG^{TR}, α-MyHC, and Gapdh mRNAs (Online Figure II and Online Table I).

Induction of Adipogenesis

C-Kit$^+$ progenitor cells from nontransgenic (NTG), PG^{WT}, and PG^{TR} mouse hearts and from PG$^{+/+}$ and PG$^{-/-}$ embryos were plated at a density of 60,000 cells per well on 0.1% gelatin-coated cover glass and treated with Adipogenesis Induction Medium (α-MEM supplemented with 10% FBS, 1% antibiotic–antimycotic, 10 μg/mL insulin, 0.5 mmol/L 3-isobutyl-1-methylxanthine, and 1 μmol/L dexamethasone) for 5 days. The media was then changed to Maintenance Medium containing 10 μg/mL insulin. Two days later, cells were stained with ORO and C/EBP-α.

To quantify the number of adipocytes, the number of ORO-stained cells in 25 microscopic fields (4× magnification) and the number of C/EBPα-stained cells in 20 fields (63× magnification) per group were counted in 3 independent experiments.

Activation of Wnt Signaling by Pharmacological Inhibition of GSK-3β

CPCs from the heart of PG^{TR} mice were plated on 0.1% gelatin-coated cover glass in proliferation media, supplemented with 2 μmol/L, 5 μmol/L, and 10 μmol/L of 6-bromoindirubin-3′-oxime (BIO), a known activator of the canonical Wnt signaling.[23] Untreated cells and cells treated with BIO but not subjected to adipogenesis were included as control groups. At the end of the treatment, cells were stained with ORO and C/EBP-α, and the percentages of positive cells were determined.

Real-Time PCR (qPCR)

Levels of mRNAs for selected molecular markers were quantified by qPCR using specific TaqMan Gene expression assays (Online Table I) and were normalized to Gapdh mRNA level.

Statistical Analysis

Statistical analysis was performed using STATA-Intercooled version 10.1 software (StataCorp LP, College Station, TX), as described.[15] Data are expressed as mean ±1 SD. Kaplan–Meier survival curves were compared by log-rank test.

An expanded Methods section can be found online at http://circres.ahajournals.org.

Results

Cardiac Lineage-Specific Expression of PG Leads to Increased Fibroadiposis, Cardiac Dysfunction, and Premature Death

We generated 2 lines of PG^{WT} and 3 lines of PG^{TR} transgenic mice using a 5.5-kbp α-MyHC promoter (a generous gift from Dr. Jeffrey Robbins, University of Cincinnati). The 11 novel amino acids in the PG^{TR} were used as an epitope to generate mutant PG-specific (PG^{TR}) antibody (Figure 1A). The custom-made antibody against this epitope reacted with PG^{TR} but not PG^{WT} (Online Figure I). Expression of the transgene protein in the heart was detected using Flag-specific (PG^{WT}), PG^{TR}-specific, and pan PG (transgene PG + PG^{Endo}) antibodies (Figure 1B). Relative expression levels of the PG^{WT} and PG^{TR}, quantified after probing the membranes with a Pan PG antibody, were 31% to 41% and 26% to 47% of total PG, respectively (Figure 1B and C). Lines with the higher expression of the transgene (41% in PG^{WT} and 47% in PG^{TR}) were used for further characterization.

Six- to 12-month-old NTG, PG^{WT}, and PG^{TR} mice were euthanized for morphological and histological characterization. Hearts were enlarged in PG^{TR} mice in comparison with NTG or PG^{WT} mice (Figure 2A). The ventricular/body weight ratio was significantly increased in age- and sex-matched PG^{TR} mice in comparison with NTG mice (5.1±1.1 versus 4.4±0.5 mg/g, respectively, P=0.006) or PG^{WT} (4.5±0.6 mg/g, P=0.015). The ventricular/body weight ratio was not significantly different between PG^{WT} and NTG mice (Figure 2B). Histological examination showed increased number of adipocytes in the heart in PG^{WT} and PG^{TR} mice. (NTG: 0.19%±14%, PG^{WT}: 0.63%±0.23%, PG^{TR}: 0.60%±19% of total cells; 4060 cells per mouse and 3–4 mice per group, P<0.001.) Distribution of adipocytes in the myocardium was patchy and predominantly at the epicardium (Figure 2C). The number of adipocytes did not seem to differ significantly between the right and left ventricles, in accord with the expected expression of the transgenes regulated by the α-MyHC promoter in both ventricles. Likewise, interstitial fibrosis was increased by approximately 2-fold in the PG^{WT} and PG^{TR} mice, in comparison with NTG.

PG^{WT} and PG^{TR} mice exhibited increased mortality in comparison with NTG mice. Approximately 10%, 20%, and 60% of PG^{TR} died at 6, 12, and 24 months of age, respectively (Figure 2D). Echocardiographic findings are presented in Table. Left ventricular end diastolic diameter (LVEDD), end systolic diameter (ESD), and mass (LVM) were increased and LV fractional shortening (LVFS) was decreased in the PG^{TR} mice. PG^{WT} mice showed a modest increase in LVEDD but had normal LVESD and preserved LVFS. Electrocardiograms showed evidence of third-degree atrioventricular (AV) block, supraventricular tachycardia, AV dissociation, and ventricular arrhythmias in transgenic mice (Online Table II and Online Figure III).

To recapitulate the human genotype, we attempted to generate mice that expressed only PG^{TR} in the heart. However, expressing PG^{TR} in the background of homozygous deficiency of PG^{Endo} ($PG^{-/-}$:PG^{TR}) did not produce viable pups, presumably because of early lethality of $PG^{-/-}$ embryos. [21] Bigenic mice expressing PG^{TR} in the background of heterozygous deficiency of PG^{Endo} ($PG^{\pm}$:PG^{TR}) were viable and exhibited a phenotype similar to that observed in the PG^{TR} transgenic mice, including increased fibroadipocytes (Online Figure

IV). Echocardiographically, the bigenic $PG^{\pm}$:PG^{TR} mice showed increased LVEDD, LVESD, and LVM and reduced LVFS (Online Table III). Heterozygous deficiency of PG ($PG^{\pm}$) was also associated with increased LVEDD, but these mice had preserved LVFS. In comparison with $PG^{\pm}$ mice, the bigenic $PG^{\pm}$:PG^{TR} mice exhibited significantly increased LVEDD, LVESD, and LVM and significantly lower LVFS (Online Table III).

Impaired Binding of Mutant PG^{TR} to Other Desmosome Proteins, Reduced Desmosome Incorporation, and Enhanced Nuclear Localization

Immunoreactive signal for PG^{TR} was virtually absent at desmosomal sites and was primarily detected in the nucleus (Figure 3A). However, PG^{WT} was detected in the desmosome as well as in the nucleus.

Immunoblotting of cell protein subfractions showed findings consistent with the results of the immunofluorescence staining. Accordingly, PG^{WT} and PG^{TR} were detected in the nuclear and cytosolic protein subfractions. PG^{WT} was also present in the membrane subfraction. In contrast, PG^{TR} was minimally detectable in the membrane subfraction (Figure 3B).

Co-IP studies (Figure 3C) showed reduced binding of PG^{TR} to its interacting desmosome proteins DSP and DSG2, but preserved binding to DSC-2. In contrast, binding of PG^{WT} to DSP, DSG2, and DSC2 was preserved (Figure 3C). Likewise, both PG^{WT} and PG^{TR} were coprecipitated with TCF7l2 (Figure 3D).

Enhanced Adipogenesis in CPCs Isolated from PG^{WT} or PG^{TR}

To test the direct role of PG in adipogenesis, we isolated c-Kit^+/$Sca1^+$, c-Kit^+, and $Sca1^+$ cells from the hearts of age- and sex-matched NTG, PG^{WT}, and PG^{TR} adult mice by FACS. C-Kit^+:$Sca1^+$ cells comprised about 0.1%±0.08% of cardiac myocytes depleted cell pools in the hearts in 4 independent isolations. The relatively high percentage of c-Kit^+:$Sca1^+$ cells, while in accord with some of the previous data,[24,25] likely reflects our 2-step gating enrichment strategy (Online Figure V). The percentage does not reflect the number of c-Kit^+:$Sca1^+$ cells in vivo in the myocardium, which is expected to be much lower. There were no significant differences in the number of c-Kit^+:$Sca1^+$ isolated from NTG, PG^{WT}, and PG^{TR} mouse hearts.

RT-PCR, performed using specific primers (Online Figure II and Online Table I), showed expression of PG^{Endo} in CPCs isolated from NTG, PG^{WT}, and PG^{TR} mouse hearts (Figure 4A). Likewise, PG^{WT} and PG^{TR} were expressed in c-Kit^+:$Sca1^+$ cells isolated from the hearts of PG^{WT} and PG^{TR} mice, respectively. In addition, α-MyHC was also expressed in the isolated CPCs (Figure 4A). The latter finding also corroborated expression of the PG transgenes regulated by the α-MyHC promoter.

Immunofluorescence staining of c-Kit^+:$Sca1^+$ cells with specific antibodies against PG^{TR}, PG^{WT}, and pan PG also confirmed expression of the PG in CPCs and suggested nuclear localization of transgene PG in these cells (Figure 4B and 4C). Moreover, immunofluorescence staining for PG and c-Kit^+, performed without cell permeabilization in order to preserve the transmembrane antigen c-Kit, confirmed coexpression of c-Kit and PG in CPCs (Figure 4C).

To determine whether expression of PG in CPCs enhanced adipogenesis, we stimulated c-Kit^+:$Sca1^+$ cells isolated from NTG, PG^{WT}, and PG^{TR} hearts for adipogenesis and stained with ORO and C/EBP-α. CPCs isolated from PG^{WT} and PG^{TR} mice showed increased accumulation of fat droplets as well as a higher number of C/EBP-α expressing cells (Figure 5A), in comparison with NTG cells. Numbers of ORO and C/EBP-α positive cells are shown

in Figure 5B and 5C. In addition, c-Kit$^+$ but Sca1$^-$ cells isolated from PG^{TR} mouse hearts also showed enhanced adipogenesis (Online Figure VIA and VIB). Moreover, CPCs isolated from PG^{TR} and PG^{WT} but not from NTG mice exhibited spontaneous adipogenesis in the absence of an adipogenic induction (Figure 5D through 5F).

To determine a transcriptional switch to adipogenesis regulated by the canonical Wnt signaling, we performed qPCR to quantify mRNA levels of KLF15, IGFBP5, and CTGF.[26,27] KLF15 and IGFBP5 mRNA levels were increased markedly (3–5-fold and 105–144-fold, respectively) in PG^{WT} and PG^{TR} progenitor cells (Figure 5G). Likewise, mRNA level of Wnt5B, a noncanonical Wnt that promotes adipogenesis[28] was increased significantly. In contrast, mRNA level of CTGF, a known inhibitor of adipogenesis and a target of the canonical Wnt signaling,[29] was significantly reduced.

To further substantiate suppressed canonical Wnt signaling by PG in mediating adipogenesis in CPCs, we activated the canonical Wnt signaling by treating c-Kit$^+$:Sca1$^+$ cells with BIO, a known inhibitor of GSK3α.[23] Cyclin D1 and c-Myc mRNA levels, targets of the canonical Wnt signaling, were reduced in c-Kit$^+$:Sca1$^+$ cells isolated from PG^{TR} hearts but treated with BIO, indicating suppressed canonical Wnt signaling (Figure 6A). Treatment with BIO normalized cyclin D1, c-Myc, and CTGF mRNA levels in c-Kit$^+$:Sca1$^+$ cells isolated from PG^{TR} hearts (Figure 6A). In accord with molecular rescue of the canonical Wnt targets, treatment with increasing concentrations of BIO reversed adipogenesis in c-Kit$^+$:Sca1$^+$ cells in a dose-dependent manner, despite treatment with adipogenic inducers (Figure 6B through 6D). In contrast, CPCs not treated with BIO showed enhanced adipogenesis. Similar experiments in c-Kit$^+$ only cells isolated from PG^{TR} hearts replicated the findings in c-Kit$^+$:Sca1$^+$ cells on reversal of adipogenesis with BIO (Online Figure VIC and VID).

Resistant of PG$^{-/-}$ CPCs to Adipogenesis

PG$^{+/+}$ and PG$^{-/-}$ c-Kit$^+$ CPCs, isolated from E11 embryos (Online Figure VII and Online Table I) were morphologically identical (Figure 7A). Mouse embryonic fibroblasts (MEFs) isolated from PG$^{+/+}$ and PG$^{-/-}$ embryos showed differential adipogenesis when subjected to adipogenic induction. MEFs from PG$^{-/-}$ showed about 20-fold reduction in the number of ORO stained cells in comparison with PG$^{+/+}$ cells (Online Figure VIII).

The number of c-Kit$^+$ cells (Lin$^-$ and Flk1$^-$) was significantly reduced in the PG$^{-/-}$ embryos in comparison with PG$^{+/+}$ embryos. Representative plots showing the gating setting used to identify and sort Lin$^-$:Flk1$^-$:c-Kit$^+$ cells are shown in Figure 7B. On average, c-Kit$^+$ cells represented about 2% to 8% of the Lin$^-$:Flk1$^-$ cells in the PG$^{+/+}$ embryos, in contrast to 0.1% to 1.5% of the Lin$^-$:Flk1$^-$ cells in the PG$^{-/-}$ embryos, a several-fold reduction. In addition, PG$^{-/-}$ CPCs were resistant to adipogenesis, because only rare ORO positive cells were found despite adipogenic induction. In contrast, adipogenesis was effectively induced in the PG$^{+/+}$ CPCs (Figure 7C and 7E). Consistent with resistance to adipogenesis, mRNA level of CTGF, an inhibitor of adipogenesis,[27] was increased by 22-fold in PG$^{-/-}$:c-Kit$^+$ CPCs (Figure 7F). To determine whether resistance to adipogenesis in PG$^{-/-}$:c-Kit$^+$ CPCs was associated with activation of canonical Wnt signaling, we measured mRNA levels of Sox2, c-Myc, and cyclin D1, downstream targets of this pathway and cyclin E1 and PCNA, markers of cell proliferation. Sox2, c-Myc, and cyclin D1 as well as cyclin E1 and PCNA mRNA levels were increased significantly (Figure 7F). Collectively, these data link inhibition of adipogenesis in PG$^{-/-}$:c-Kit$^+$ CPCs to activation of the canonical Wnt signaling.

Discussion

The findings provide direct evidence for the essential signaling functions of nuclear PG in repressing the Wnt/β-catenin signaling pathway in CPCs and inducing a transcriptional switch to adipogenesis in ARVC. In the presence of PG, c-kit1^{+}:Sca1^{+} CPCs exhibited enhanced differentiation to adipocytes. In contrast, in the absence of PG these cells were resistant to adipogenesis. These findings in conjunction with previous data in cardiac myocytes-restricted Dsp-deficient mice and genetic fate mapping experiments[14,15] identify PG as a mediator of differentiation of a subset of CPCs from a myogenic to an adipogenic fate in ARVC. We expressed PG in CPCs under the transcriptional regulation of *Myh6*, which is conventionally considered a postnatal gene. However, *Myh6* is also expressed during early embryonic period and in c-kit^{+} CPCs.[30,31] In support of the embryonic expression of *Myh6*, cardiac myocytes lineage-restricted deletion of *Dsp* under the transcriptional regulation of the α-MyHC promoter leads to near total embryonic lethality at E12–14.[14] Notwith-standing the existing data, we detected expressions of α-MyHC and PG, regulated by *Myh6* promoter, in CPCs isolated from PG^{WT} and PG^{TR}. Coexpression of PG and α-MyHC in c-Kit^{+} cells indicates a subset of cells that are in transition from a progenitor state to an early myogenic lineage.

Unlike our transgenic PG^{WT} model, PG is not overexpressed in human ARVC. We overexpressed PG^{WT} in the heart in order to determine the signaling functions of PG that is not incorporated into desmosomes (nonjunctional PG), as in human ARVC, PG is displaced from the junction.[20] We placed a Flag epitope to track and distinguish the transgene PG^{WT} from the endogenous PG. Co-IP and immunofluorescence studies showed proper desmosome localization and binding of Flag-tagged PG to selected desmosome proteins. Unlike the PG^{WT}, the mutant PG^{TR} was not epitope tagged, because of generation of a PG^{TR}-specific antibody. The PG^{WT} and PG^{TR} both exhibited excess fibroadipocytes, suggesting that the observed phenotype is not because of the Flag epitope. Furthermore, we and others have previously shown that nontagged endogenous PG could translocate to nucleus, suppress the canonical Wnt signaling, and provoke adipogenesis.[14] Nevertheless, we also generated bigenic PG$^{\pm}$:PG^{TR} mice, which exhibited excess fibroadipocytes in the heart and cardiac dysfunction, as also observed in the single transgenic PG^{TR} mice. Collectively, these data indicate that findings reflect signaling functions of PG.

PG^{TR} transgenic mice express a truncated PG, known to cause Naxos disease in humans.[11] The PG^{TR} transgenic mice exhibit a phenotype that resembles ARVC. However, the genotype of PG^{TR} mice is not identical to the genotype of humans as Naxos disease is caused a homozygous deletion mutation in PG. Expression of PG^{TR} under the transcriptional control of *Myh6* did not rescue early embryonic lethality of PG deficiency,[21] indicating earlier expression of PG than *Myh6*. The PG$^{\pm}$:PG^{TR} mice, however, exhibited a phenotype similar to PG^{TR} mice. Nevertheless, because of the differences in the genotypes of mouse models and human patients, application of the findings to human ARVC remains to be determined. In addition, the findings may not pertain to the pathogenesis of ARVC caused by genes coding for nondesmosome proteins or various phenotypic features of ARVC, such as gap junction remodeling, cardiac arrhythmias, and myocardial fibrosis, which may result from interactions of PG with other cellular proteins, not analyzed in the present study. Finally, alternative approaches to activate the canonical Wnt signaling, other than inhibition of GSK3β with BIO, might provide further insights.

Cardiac dysfunction in PG^{TR} and PG$^{\pm}$:PG^{TR} was similar and likely results from poor assembly of the truncated PG into desmosome, reflected by reduced levels of PG^{TR} in cell membrane. In contrast, PG^{WT} mice exhibited only mild left ventricular dilatation. Despite disparities in cardiac dysfunction, PG^{TR} and PG^{WT} mice exhibited premature mortality and

cardiac arrhythmias. The molecular mechanisms responsible for cardiac arrhythmias and increased mortality in PG^{WT} remain to be explored. The findings also suggest partial dissociation of cardiac dysfunction from fibroadipogenesis in ARVC, as the former primarily reflects impaired desmosome assembly at least in early stages of ARVC, and the latter differentiation of CPCs to adipocytes. In advances stages of ARVC, adipocytes infiltration of the myocardium might also contribute to cardiac dysfunction.[2]

PG seems to regulate—probably through the canonical Wnt pathway—expression of several adipogenic factors. Changes in CTGF mRNA level inversely paralleled expression of PG. CTGF, also known as CCN2, is a known target of the canonical Wnt signaling[29] and yet regulates Wnt signaling by interacting with Wnt coreceptor, LRP6.[32] These data identify CTGF as a plausible molecular mediator of adipogenesis in ARVC. Likewise, expression level of KLF15, known to inhibit cardiac myocytes hypertrophy and repress transcriptional activator myocardin,[33,34] was significantly increased in PG^{+} CPCs. KLF15 is highly expressed in brown adipose tissue and is markedly up-regulated during differentiation of preadipocytes to adipocytes.[26] KLF15 is also known to inhibit CTGF in cardiac fibroblasts.[35] Moreover, IGFBP5 mRNA level was increased by more than 100-fold in CPCs that expressed PG. IGFBP5 is a target of Akt1/FOXO transcription factors and also is regulated by the Wnt/β-catenin signaling pathway (reviewed by Beattie et al[36]). IGFBP5 is implicated in a diverse array of biological functions, including muscle atrophy, cell senescence, survival, and differentiation as well as fibrosis and inflammatory response through IGF-1-dependent and -independent mechanisms (reviewed by Beattie et al[36]). While these biological processes have been implicated in the pathogenesis of ARVC, specific biological roles of IGFBP5 in ARVC, and the molecular basis of increased mRNA levels merit additional studies. Additional interventions targeted to CTGF, KLF15, and IGBP15 in animal models of ARVC would be necessary to substantiate the essential roles of these molecules in the pathogenesis of ARVC.

In summary, through a series of gain- and loss-of-function studies, we have shown the central role of nuclear PG in mediating adipogenesis of ARVC and identified CTGF, KLF15, IGFBP5, and Wnt5b as potential mediators of the unique and enigmatic phenotype in ARVC. These data in conjunction with our previous studies in *Dsp*-deficient mice and genetic fate mapping studies[14,15] highlight the signaling functions of nuclear PG in repressing the canonical Wnt signaling and mediating differentiation of a subset of $c\text{-}Kit^{+}$ CPCs to adipocytes.

Novelty and Significance

What Is Known?

- Arrhythmogenic right ventricular cardiomyopathy (ARVC), an important cause of sudden cardiac death in the young, is an enigmatic disease characterized by fibroadipocytic replacement of cardiac myocytes, particularly in the right ventricle.
- Mutations in genes encoding desmosome proteins are responsible for at least 50% of the ARVC cases.
- Partial nuclear displacement of plakoglobin (PG) from desmosomes leading to suppression of the canonical Wnt signaling in the second heart field cardiac progenitor cells (CPCs) is a putative mechanism for ARVC.

What Is New?

- The $c\text{-}Kit^{+}$ CPCs isolated from the heart of transgenic mouse models of ARVC expressed PG, exhibited suppressed canonical Wnt signaling, and showed

enhanced adipogenesis. Activation of the canonical Wnt signaling rescued the adipogenic phenotype.

- In contrast, c-Kit$^+$ CPCs isolated from PG null embryos showed activation of the canonical Wnt signaling and were resistant to adipogenesis.
- CTGF, KLF15, Wnt5b, and IGFBP5 were transcriptional switch regulators of adipogenesis targeted by the PG-canonical Wnt signaling pathway in the c-Kit$^+$ CPCs.

These findings provide insights into the molecular pathogenesis of ARVC and implicate the signaling functions of nuclear PG as a responsible mechanism. Our studies show that in AVRC, nonjunctional PG translocates to the nucleus where it activates a transcriptional program that switches the differentiation of c-Kit$^+$ CPCs from a myogenic to an adipogenic fate.

Supplementary Material

Refer to Web version on PubMed Central for supplementary material.

Non-Standard Abbreviations and Acronyms

α-MyHC	α-myosin heavy chain
ARVC	arrhythmogenic right ventricular cardiomyopathy
bFGF	basic fibroblast growth factor
BIO	6-bromoindirubin-3′-oxime
C/EBP-α	CCAAT/enhancer binding protein
CPCs	cardiac progenitor cells
CTGF	connective tissue growth factor
DSC2	desmocollin 2
DSG2	desmoglein 2
DSP	desmoplakin
FACS	fluorescence activated cell sorting
GSK-3β	glycogen synthase kinase 3 β
IGFBP5	insulin growth factor binding protein 5
KLF15	kruppel-like factor 15
mLIF	mouse leukemia inhibitory factor
NTG	nontransgenic
PG	plakoglobin
PG^{Endo}	endogenous PG
PG^{TR}	truncated PG
PG^{WT}	wildtype PG
PKP2	plakophillin 2

Acknowledgments

The authors wish to acknowledge Mr. Prejusa Allan for his technical support with FACS of CPCs.

Sources of Funding

Supported in part by grants from the NHLBI (R01-088498 and R21 AG038597), Burroughs Wellcome Award in Translational Research (1005907.01), and a TexGen grant from Greater Houston Community Foundation.

References

1. Basso C, Corrado D, Marcus FI, Nava A, Thiene G. Arrhythmogenic right ventricular cardiomyopathy. Lancet. 2009; 373:1289–1300. [PubMed: 19362677]
2. Delmar M, McKenna WJ. The cardiac desmosome and arrhythmogenic cardiomyopathies: from gene to disease. Circ Res. 2010; 107:700–714. [PubMed: 20847325]
3. Lombardi R, Marian AJ. Molecular genetics and pathogenesis of arrhythmogenic right ventricular cardiomyopathy: a disease of cardiac stem cells. Pediatr Cardiol. 2011; 32:360–365. [PubMed: 21267716]
4. Frank R, Fontaine G, Vedel J, Mialet G, Sol C, Guiraudon G, Grosgogeat Y. Electrocardiology of 4 cases of right ventricular dysplasia inducing arrhythmia. Archives des Maladies du Coeur et Des Vaisseaux. 1978; 71:963–972. [PubMed: 102297]
5. van Tintelen JP, Entius MM, Bhuiyan ZA, Jongbloed R, Wiesfeld AC, Wilde AA, van der SJ, Boven LG, Mannens MM, van Langen IM, Hofstra RM, Otterspoor LC, Doevendans PA, Rodriguez LM, van Gelder IC, Hauer RN. Plakophilin-2 mutations are the major determinant of familial arrhythmogenic right ventricular dysplasia/cardiomyopathy. Circulation. 2006; 113:1650–1658. [PubMed: 16567567]
6. Pilichou K, Nava A, Basso C, Beffagna G, Bauce B, Lorenzon A, Frigo G, Vettori A, Valente M, Towbin J, Thiene G, Danieli GA, Rampazzo A. Mutations in desmoglein-2 gene are associated with arrhythmogenic right ventricular cardiomyopathy. Circulation. 2006; 113:1171–1179. [PubMed: 16505173]
7. Awad MM, Dalal D, Cho E, Amat-Alarcon N, James C, Tichnell C, Tucker A, Russell SD, Bluemke DA, Dietz HC, Calkins H, Judge DP. Dsg2 mutations contribute to arrhythmogenic right ventricular dysplasia/cardiomyopathy. Am J Hum Genet. 2006; 79:136–142. [PubMed: 16773573]
8. Gerull B, Heuser A, Wichter T, Paul M, Basson CT, McDermott DA, Lerman BB, Markowitz SM, Ellinor PT, MacRae CA, Peters S, Grossmann KS, Michely B, Sasse-Klaassen S, Birchmeier W, Dietz R, Breithardt G, Schulze-Bahr E, Thierfelder L. Mutations in the desmosomal protein plakophilin-2 are common in arrhythmogenic right ventricular cardiomyopathy. Nat Genet. 2004; 36:1162–1164. [PubMed: 15489853]
9. Alcalai R, Metzger S, Rosenheck S, Meiner V, Chajek-Shaul T. A recessive mutation in desmoplakin causes arrhythmogenic right ventricular dysplasia, skin disorder, and woolly hair. J Am Coll Cardiol. 2003; 42:319–327. [PubMed: 12875771]
10. Rampazzo A, Nava A, Malacrida S, Beffagna G, Bauce B, Rossi V, Zimbello R, Simionati B, Basso C, Thiene G, Towbin JA, Danieli GA. Mutation in human desmoplakin domain binding to plakoglobin causes a dominant form of arrhythmogenic right ventricular cardiomyopathy. Am J Hum Genet. 2002; 71:1200–1206. [PubMed: 12373648]
11. McKoy G, Protonotarios N, Crosby A, Tsatsopoulou A, Anastasakis A, Coonar A, Norman M, Baboonian C, Jeffery S, McKenna WJ. Identification of a deletion in plakoglobin in arrhythmogenic right ventricular cardiomyopathy with palmoplantar keratoderma and woolly hair (naxos disease). Lancet. 2000; 355:2119–2124. [PubMed: 10902626]
12. Merner ND, Hodgkinson KA, Haywood AFM, Connors S, French VM, Drenckhahn JD, Kupprion C, Ramadanova K, Thierfelder L, McKenna W, Gallagher B, Morris-Larkin L, Bassett AS, Parfrey PS, Young TL. Arrhythmogenic right ventricular cardiomyopathy type 5 is a fully penetrant, lethal arrhythmic disorder caused by a missense mutation in the tmem43 gene. Am J Hum Gen. 2008; 82:809–821.
13. Beffagna G, Occhi G, Nava A, Vitiello L, Ditadi A, Basso C, Bauce B, Carraro G, Thiene G, Towbin JA, Danieli GA, Rampazzo A. Regulatory mutations in transforming growth factor-beta3

gene cause arrhythmogenic right ventricular cardiomyopathy type 1. Cardiovasc Res. 2005; 65:366–373. [PubMed: 15639475]

14. Garcia-Gras E, Lombardi R, Giocondo MJ, Willerson JT, Schneider MD, Khoury DS, Marian AJ. Suppression of canonical wnt/beta-catenin signaling by nuclear plakoglobin recapitulates phenotype of arrhythmogenic right ventricular cardiomyopathy. J Clin Invest. 2006; 116:2012–2021. [PubMed: 16823493]
15. Lombardi R, Dong J, Rodriguez G, Bell A, Leung TK, Schwartz RJ, Willerson JT, Brugada R, Marian AJ. Genetic fate mapping identifies second heart field progenitor cells as a source of adipocytes in arrhythmogenic right ventricular cardiomyopathy. Circ Res. 2009; 104:1076–1084. [PubMed: 19359597]
16. Rao TP, Kuhl M. An updated overview on Wnt signaling pathways: a prelude for more. Circ Res. 2010; 106:1798–1806. [PubMed: 20576942]
17. Maeda O, Usami N, Kondo M, Takahashi M, Goto H, Shimokata K, Kusugami K, Sekido Y. Plakoglobin (gamma-catenin) has tcf/lef family-dependent transcriptional activity in beta-catenin-deficient cell line. Oncogene. 2004; 23:964–972. [PubMed: 14661054]
18. Shimizu M, Fukunaga Y, Ikenouchi J, Nagafuchi A. Defining the roles of beta-catenin and plakoglobin in lef/t-cell factor-dependent transcription using beta-catenin/plakoglobin-null f9 cells. Mol Cell Biol. 2008; 28:825–835. [PubMed: 17984222]
19. Ross SE, Hemati N, Longo KA, Bennett CN, Lucas PC, Erickson RL, MacDougald OA. Inhibition of adipogenesis by Wnt signaling. Science. 2000; 289:950–953. [PubMed: 10937998]
20. Asimaki A, Tandri H, Huang H, Halushka MK, Gautam S, Basso C, Thiene G, Tsatsopoulou A, Protonotarios N, McKenna WJ, Calkins H, Saffitz JE. A new diagnostic test for arrhythmogenic right ventricular cardiomyopathy. N Engl J Med. 2009; 360:1075–1084. [PubMed: 19279339]
21. Ruiz P, Brinkmann V, Ledermann B, Behrend M, Grund C, Thalhammer C, Vogel F, Birchmeier C, Gunthert U, Franke WW, Birchmeier W. Targeted mutation of plakoglobin in mice reveals essential functions of desmosomes in the embryonic heart. J Cell Biol. 1996; 135:215–225. [PubMed: 8858175]
22. Lombardi R, Bell A, Senthil V, Sidhu J, Noseda M, Roberts R, Marian AJ. Differential interactions of thin filament proteins in two cardiac troponin t mouse models of hypertrophic and dilated cardiomyopathies. Cardiovasc Res. 2008; 79:109–117. [PubMed: 18349139]
23. Sato N, Meijer L, Skaltsounis L, Greengard P, Brivanlou AH. Maintenance of pluripotency in human and mouse embryonic stem cells through activation of wnt signaling by a pharmacological gsk-3-specific inhibitor. Nat Med. 2004; 10:55–63. [PubMed: 14702635]
24. Fazel S, Cimini M, Chen L, Li S, Angoulvant D, Fedak P, Verma S, Weisel RD, Keating A, Li RK. Cardioprotective c-kit+ cells are from the bone marrow and regulate the myocardial balance of angiogenic cytokines. J Clin Investig. 2006; 116:1865–1877. [PubMed: 16823487]
25. Zaruba MM, Soonpaa M, Reuter S, Field LJ. Cardiomyogenic potential of c-kit(+)-expressing cells derived from neonatal and adult mouse hearts. Circulation. 2010; 121:1992–2000. [PubMed: 20421520]
26. Mori T, Sakaue H, Iguchi H, Gomi H, Okada Y, Takashima Y, Nakamura K, Nakamura T, Yamauchi T, Kubota N, Kadowaki T, Matsuki Y, Ogawa W, Hiramatsu R, Kasuga M. Role of kruppel-like factor 15 (klf15) in transcriptional regulation of adipogenesis. Te JBiol Chem. 2005; 280:12867–12875.
27. Tan JT, McLennan SV, Song WW, Lo LW, Bonner JG, Williams PF, Twigg SM. Connective tissue growth factor inhibits adipocyte differentiation. Am J Physiol Cell Physiol. 2008; 295:C740–C751. [PubMed: 18596209]
28. Kanazawa A, Tsukada S, Kamiyama M, Yanagimoto T, Nakajima M, Maeda S. Wnt5b partially inhibits canonical wnt/beta-catenin signaling pathway and promotes adipogenesis in 3t3–l1 preadipocytes. Biochem Biophys Res Commun. 2005; 330:505–510. [PubMed: 15796911]
29. Luo Q, Kang Q, Si W, Jiang W, Park JK, Peng Y, Li X, Luu HH, Luo J, Montag AG, Haydon RC, He TC. Connective tissue growth factor (ctgf) is regulated by Wnt and bone morphogenetic proteins signaling in osteoblast differentiation of mesenchymal stem cells. J Biol Chem. 2004; 279:55958–55968. [PubMed: 15496414]

30. Cottage CT, Bailey B, Fischer KM, Avitable D, Collins B, Tuck S, Quijada P, Gude N, Alvarez R, Muraski J, Sussman MA. Cardiac progenitor cell cycling stimulated by pim-1 kinase. Circ Res. 2010; 106:891–901. [PubMed: 20075333]

31. Zelarayan LC, Noack C, Sekkali B, Kmecova J, Gehrke C, Renger A, Zafiriou MP, van der Nagel R, Dietz R, de Windt LJ, Balligand JL, Bergmann MW. Beta-catenin downregulation attenuates ischemic cardiac remodeling through enhanced resident precursor cell differentiation. Proc Natl Acad Sci U S A. 2008; 105:19762–19767. [PubMed: 19073933]

32. Mercurio S, Latinkic B, Itasaki N, Krumlauf R, Smith JC. Connective-tissue growth factor modulates Wnt signalling and interacts with the Wnt receptor complex. Development. 2004; 131:2137–2147. [PubMed: 15105373]

33. Fisch S, Gray S, Heymans S, Haldar SM, Wang B, Pfister O, Cui L, Kumar A, Lin Z, Sen-Banerjee S, Das H, Petersen CA, Mende U, Burleigh BA, Zhu Y, Pinto YM, Liao R, Jain MK. Kruppel-like factor 15 is a regulator of cardiomyocyte hypertrophy. Proc Natl AcadSciUSA. 2007; 104:7074–7079.

34. Leenders JJ, Wijnen WJ, Hiller M, van der Made I, Lentink V, van Leeuwen RE, Herias V, Pokharel S, Heymans S, de Windt LJ, Hoydal MA, Pinto YM, Creemers EE. Regulation of cardiac gene expression by klf15, a repressor of myocardin activity. JBiol Chem. 2010; 285:27449–27456. [PubMed: 20566642]

35. Wang B, Haldar SM, Lu Y, Ibrahim OA, Fisch S, Gray S, Leask A, Jain MK. The kruppel-like factor klf15 inhibits connective tissue growth factor (ctgf) expression in cardiac fibroblasts. J Mol Cell Cardiol. 2008; 45:193–197. [PubMed: 18586263]

36. Beattie J, Allan GJ, Lochrie JD, Flint DJ. Insulin-like growth factor-binding protein-5 (igfbp-5): a critical member of the igf axis. BiochemJ. 2006; 395:1–19.

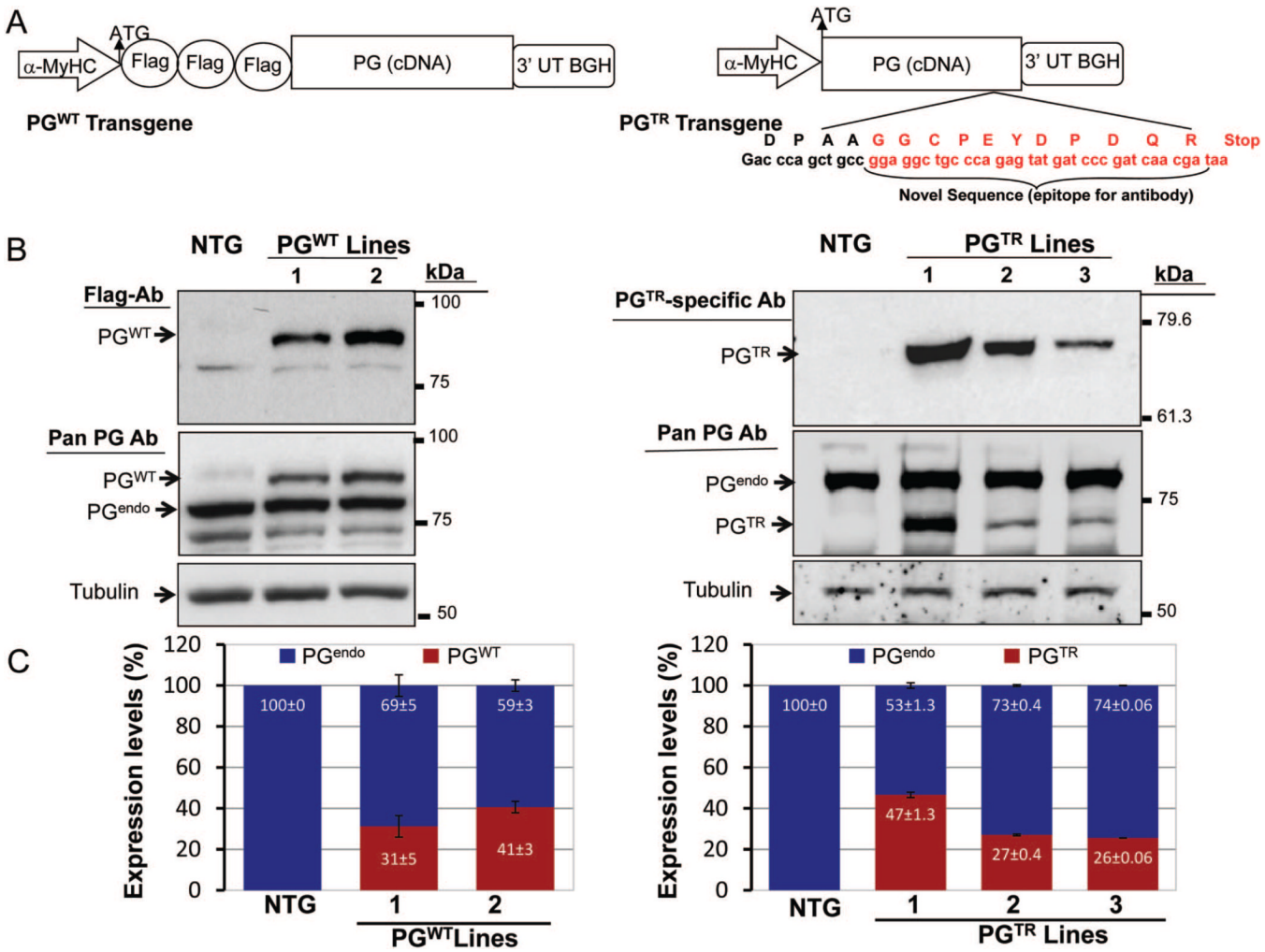

Figure 1. Transgenic mouse models

A, PG^{WT} transgene construct was generated by placing 3 Flag epitopes 5′ to full-length wild-type PG (PG^{WT}) cDNA. Truncated mutant PG (PG^{TR}) was generated by site-directed mutagenesis. The transgenes were positioned downstream to a 5.5-kbp α-MyHC promoter. **B,** Immunoblots showing expression of PG^{WT}, PG^{TR}, and PG^{Endo} proteins detected using Flag- specific (PG^{WT}), PG^{TR}-specific, and pan-PG (PG^{Endo} + PG^{WT} or + PG^{TR}) antibodies in nontransgenic (NTG) and transgenic mice. **C,** Quantitative presentation of PG^{WT} and PG^{TR} levels as percentages of the total PG in the heart of 2 lines of PG^{WT} and 3 lines of PG^{TR} mice. PG^{WT} comprised about 31% and 41% of the total PG and PG^{TR} about 47%, 27%, and 26% of total PG, respectively, in different lines analyzed.

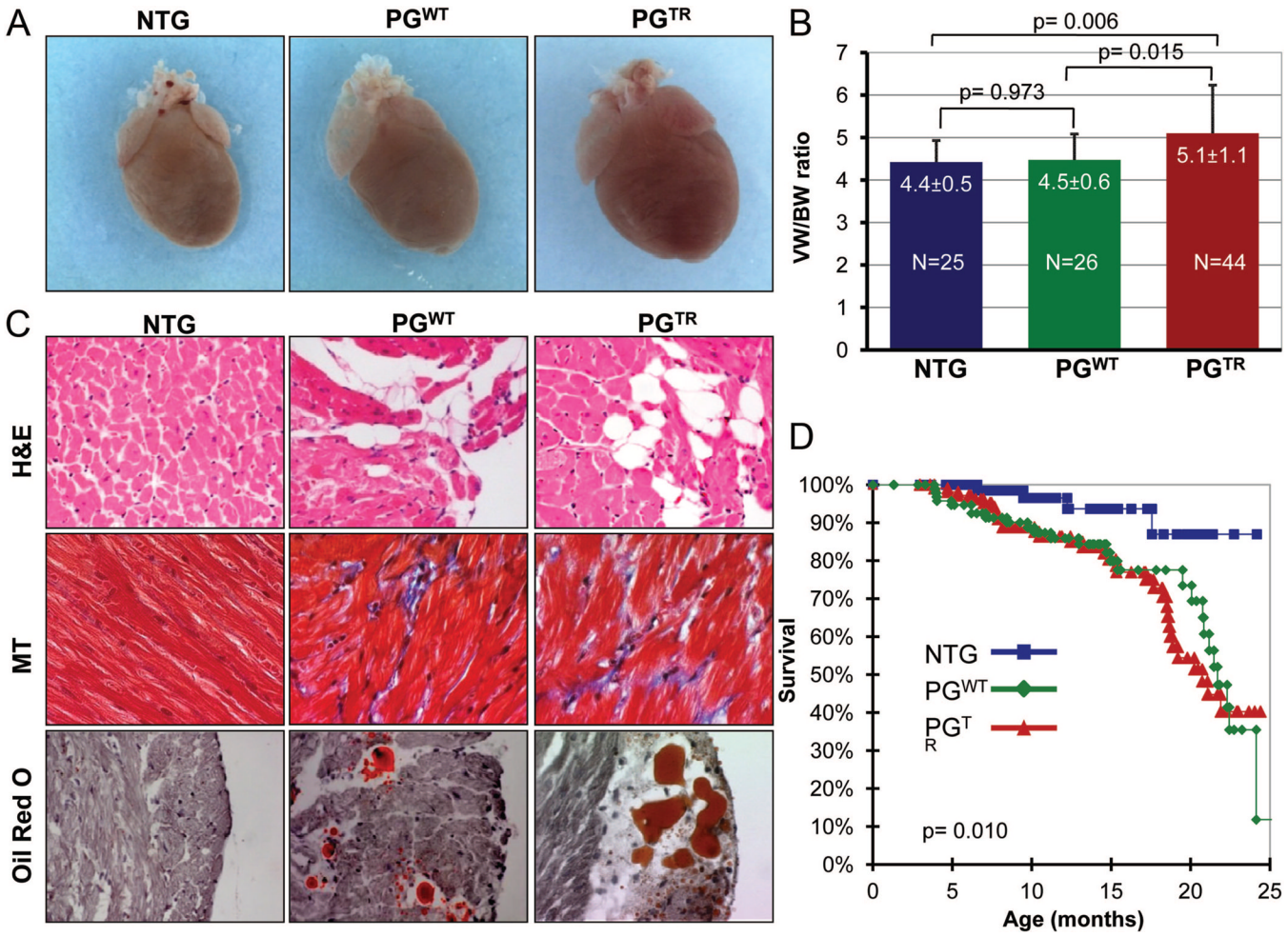

Figure 2. Cardiac phenotype in transgenic mice

A, Gross cardiac morphology of perfusion-fixed hearts showing an enlarged heart in the PG^{TR} group as compared with NTG and PG^{WT} mice. **B,** Heart/body weight ratios in the experimental groups. **C,** H&E-, Masson trichrome (MT)–, and ORO-stained thin myocardial sections showing increased fibroadiposis in the heart of PG^{WT} and PG^{TR} mice. **D,** Kaplan–Meier survival curves showing increased mortality rate in PG^{WT} and PG^{TR} mice.

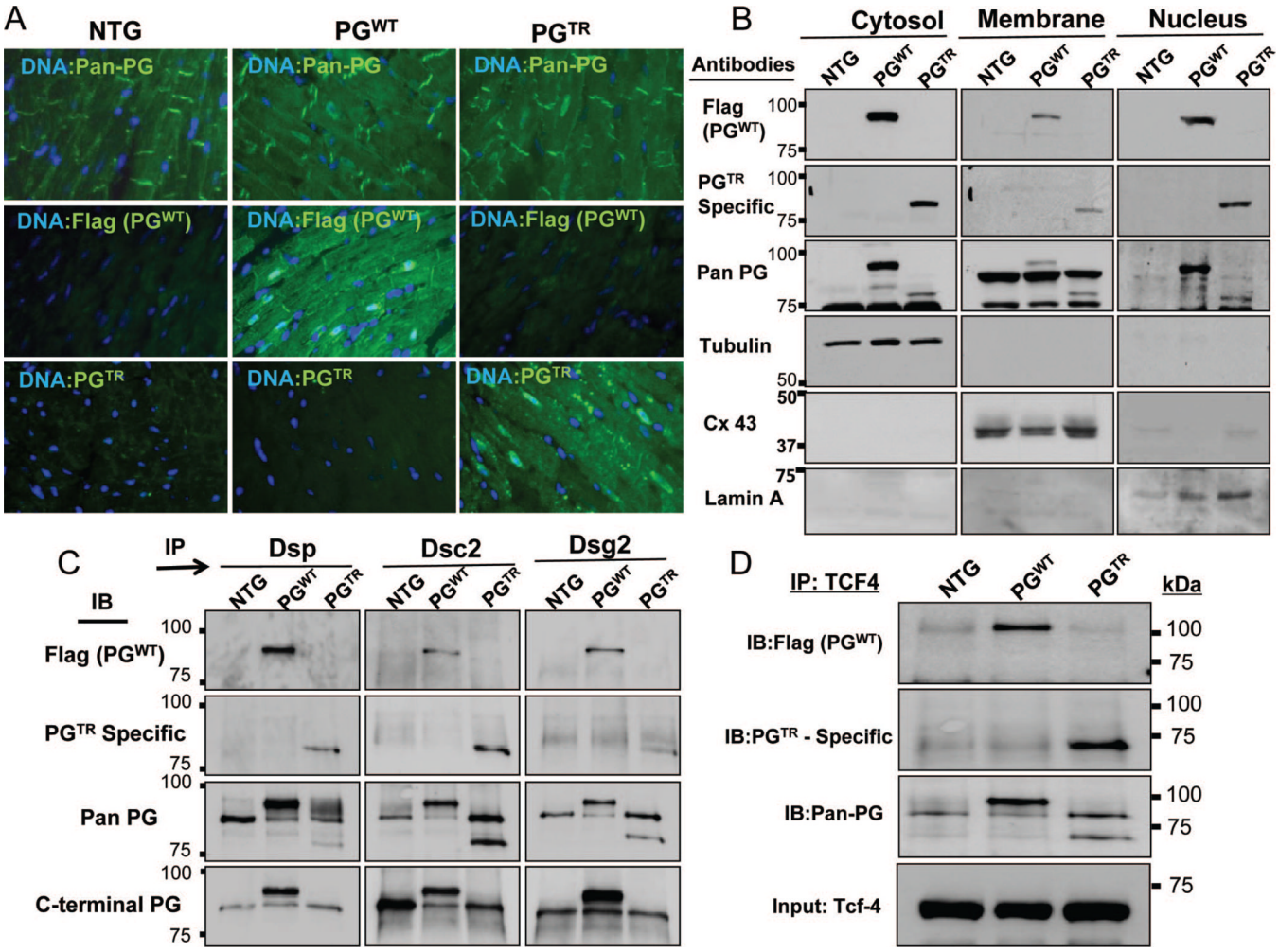

Figure 3. Desmosome incorporation, subcellular localization, and interactions with partner proteins

A, Immunofluorescence panels showing desmosome and nuclear localization of total PG, PG^{WT}, and PG^{TR}, detected using anti-pan PG, Flag, and mutant PG-specific antibodies, respectively. **B,** Immunoblots of subcellular protein fractions showing detection of PG^{WT} and PG^{TR} in the nuclear subfraction and low level of PG^{TR} in the membrane fraction, best compared in blots probed with a pan-PG antibody. **C,** Coimmunoprecipitation of PG^{Endo}, PG^{WT}, and PG^{TR} and selected protein constituents of desmosomes. Binding of PG^{TR} to Dsp and Dsg2 but not to Dsc2 was reduced. **D,** Binding of PG^{WT}, PG^{TR}, and PG^{Endo} to TCF4 transcription factor, as detected by coimmunoprecipitation.

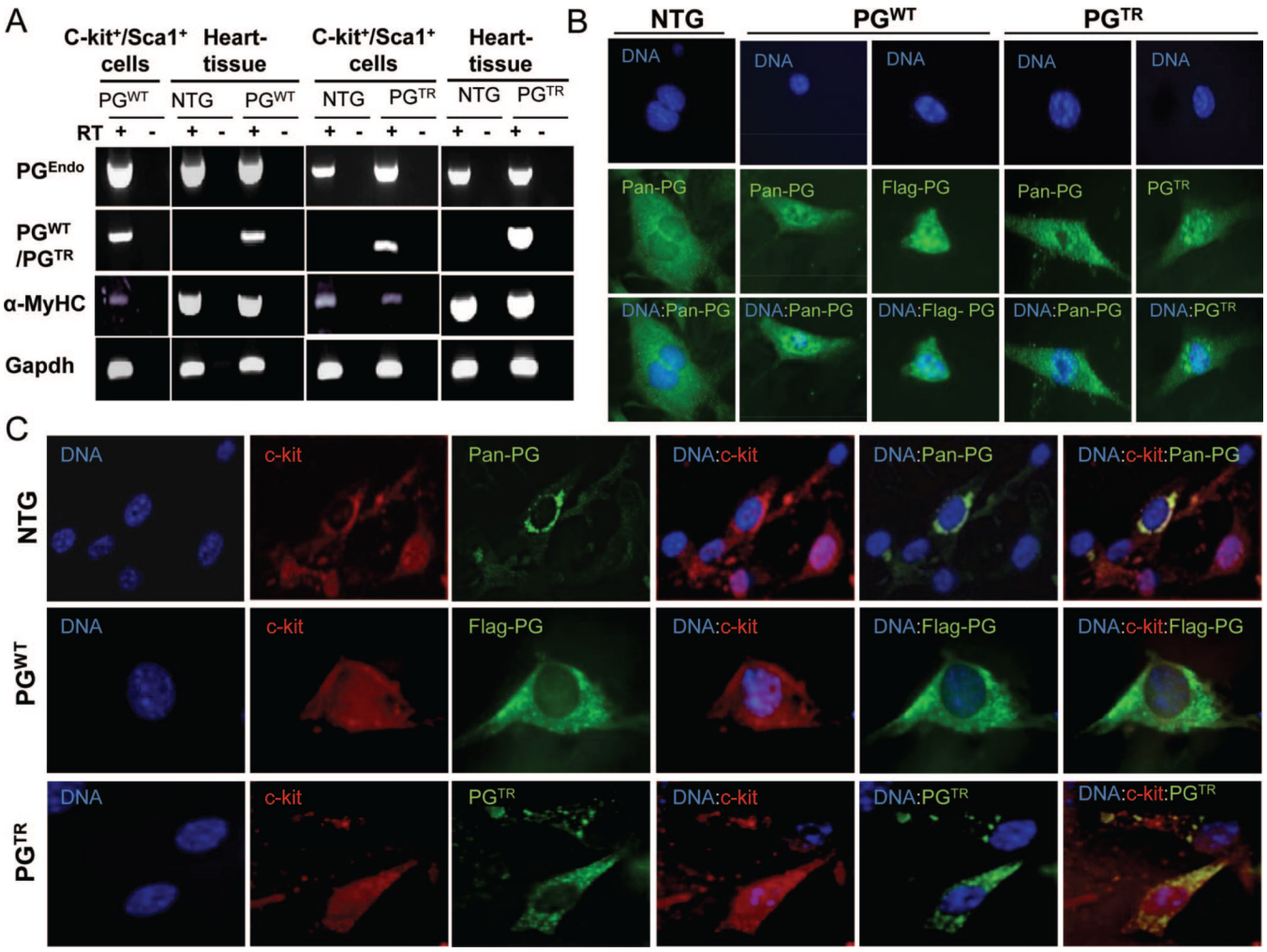

Figure 4. Detection of expression of PG in c-Kit^{+}:Sca1^{+} CPCs

A, RT-PCR panels showing expression of PG^{Endo}, PG^{WT}, PG^{TR}, and α-MyHC in c-Kit^{+}:Sca1^{+} cells isolated from the heart of NTG, PG^{WT}, and PG^{TR} mice. Heart tissue is included as a positive control. **B,** Immunofluorescence panels stained with anti-flag (PG^{WT}), PG^{TR}-specific, and pan-PG antibodies after membrane permeabilization showing expression of PG in CPCs. The panels also suggest nuclear localization of PG^{WT} and PG^{TR} in c-Kit^{+}:Sca1^{+} cells. **C,** Immunofluorescence panels showing costaining for pan PG, PG^{WT}, and PG^{TR} (**green**) along with staining for c-Kit (**red**) in CPCs.

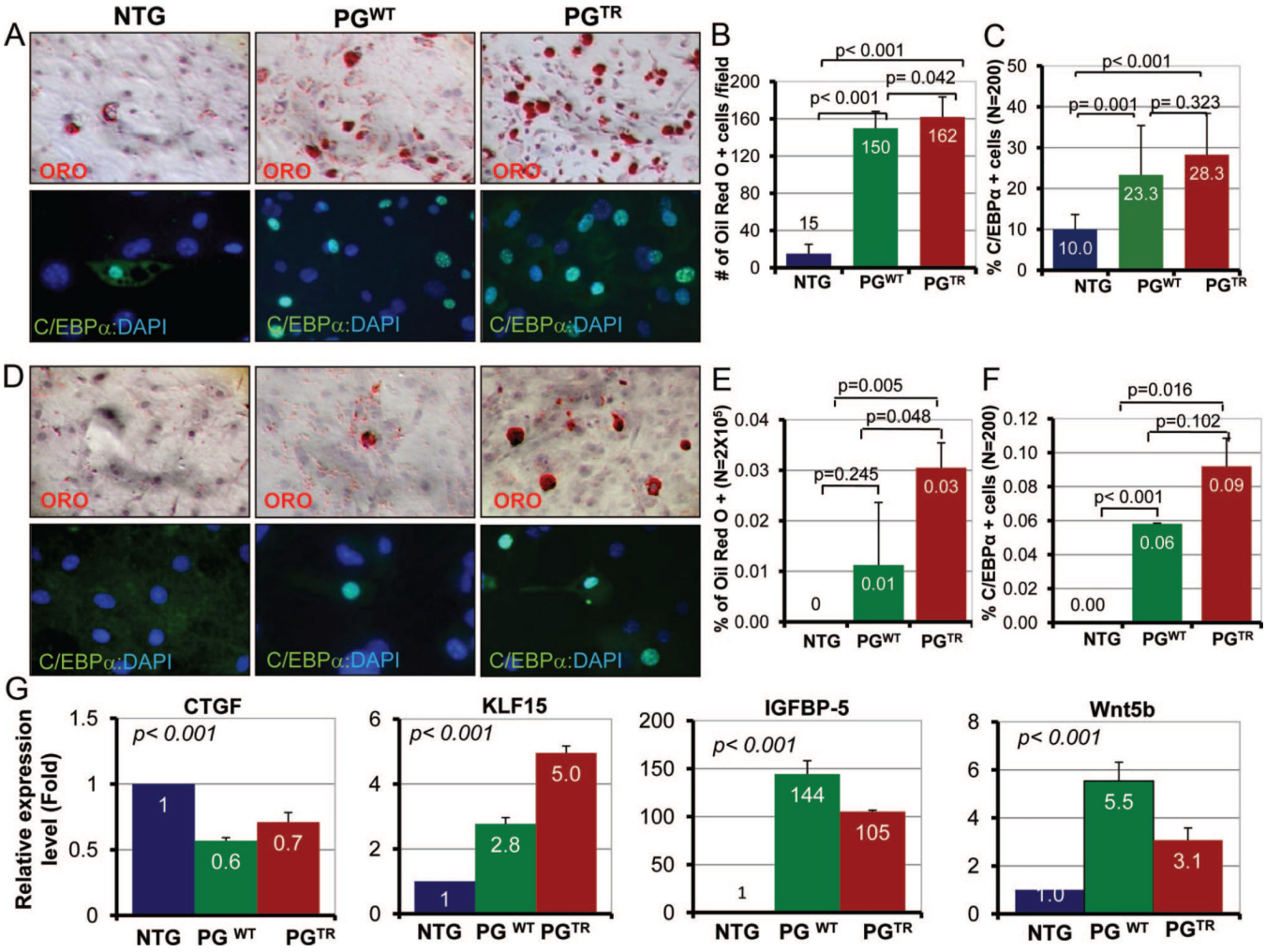

Figure 5. Adipogenesis in c-Kit$^+$:Sca1$^+$ cells

A, Represents ORO- and C/EBP-α-stained panels showing detection of fat droplets and expression of C/EBP-α in c-Kit$^+$:Sca1$^+$ cells isolated from the heart of NTG, PG^{WT}, and PG^{TR} mice. We examined 2×10^5 cells for ORO and 200 cells for C/EBP-α staining. **B,** The number of c-Kit$^+$:Sca1$^+$ cells stained positive for fat droplets was 150±18 and 162±21 cells per field in PG^{WT} an PG^{TR} groups, respectively, in comparison with 15±10 cells per field in the NTG group. **C,** Shows percentage of c-Kit$^+$:Sca1$^+$ cells that were positive for C/EBP-α expression. **D,** ORO- and C/EBP-α-stained sections showing spontaneous adipogenesis in c-Kit$^+$:Sca1$^+$ CPCs in the transgenic hearts. **E and F,** Represent quantitative assessment of ORO- and C/EBP-α-stained cells in the absence of adipogenic induction. **G,** mRNA levels of selected markers of adipogenesis in c-Kit$^+$:Sca1$^+$ cells normalized to Gapdh mRNA levels and shown relative to NTG. CTGF mRNA level, an inhibitor of adipogenesis, was reduced significantly in c-Kit$^+$:Sca1$^+$ cells in the PG^{WT} and PG^{TR} groups. In contrast, mRNA levels of KLF15 and IGFBP5 were increased dramatically. Likewise, mRNA level of Wnt5b, a noncanonical Wnt known to induced adipogenesis, was also increased significantly.

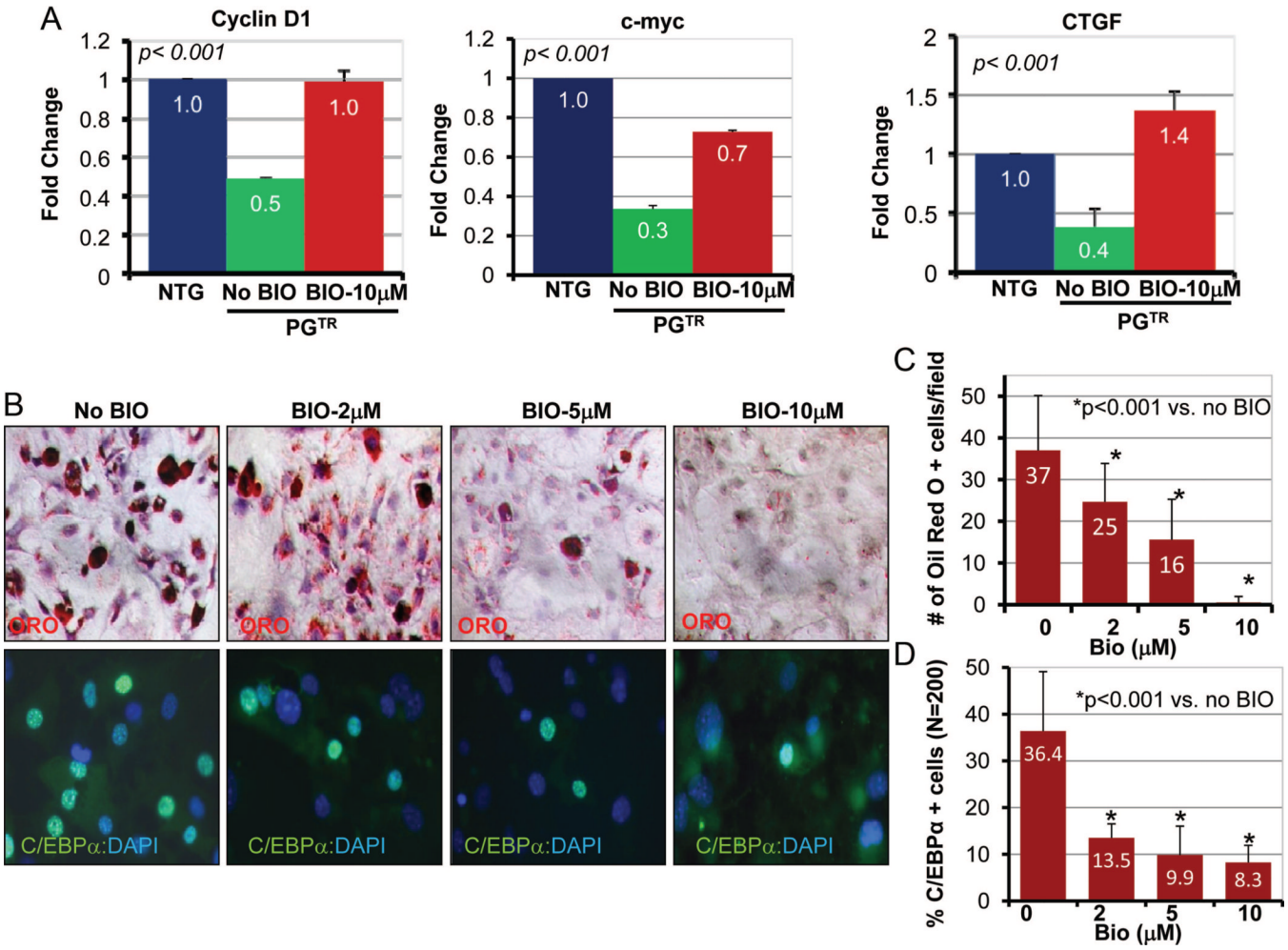

Figure 6. Rescue of adipogenesis in c-Kit$^+$:Sca1$^+$ cells on activation of the canonical Wnt signaling

A, mRNA levels of selected markers of the canonical Wnt signaling in c-Kit$^+$:Sca1$^+$ cells not treated or treated with BIO. Cyclin D1, c-Myc and CTGF mRNA levels were reduced in c-Kit$^+$:Sca1$^+$ isolated from PG^{TR} mice. Treatment with BIO normalized their mRNA levels. **B,** Treatment of c-Kit$^+$:Sca1$^+$ cells isolated from the heart of PG^{TR} mice with 3 doses of BIO prevented adipogenesis in CPCs despite adipogenic induction. **C and D,** Quantification of ORO and C/EBP-α positive cells in c-Kit$^+$:Sca1$^+$ cells treated with BIO and untreated cells.

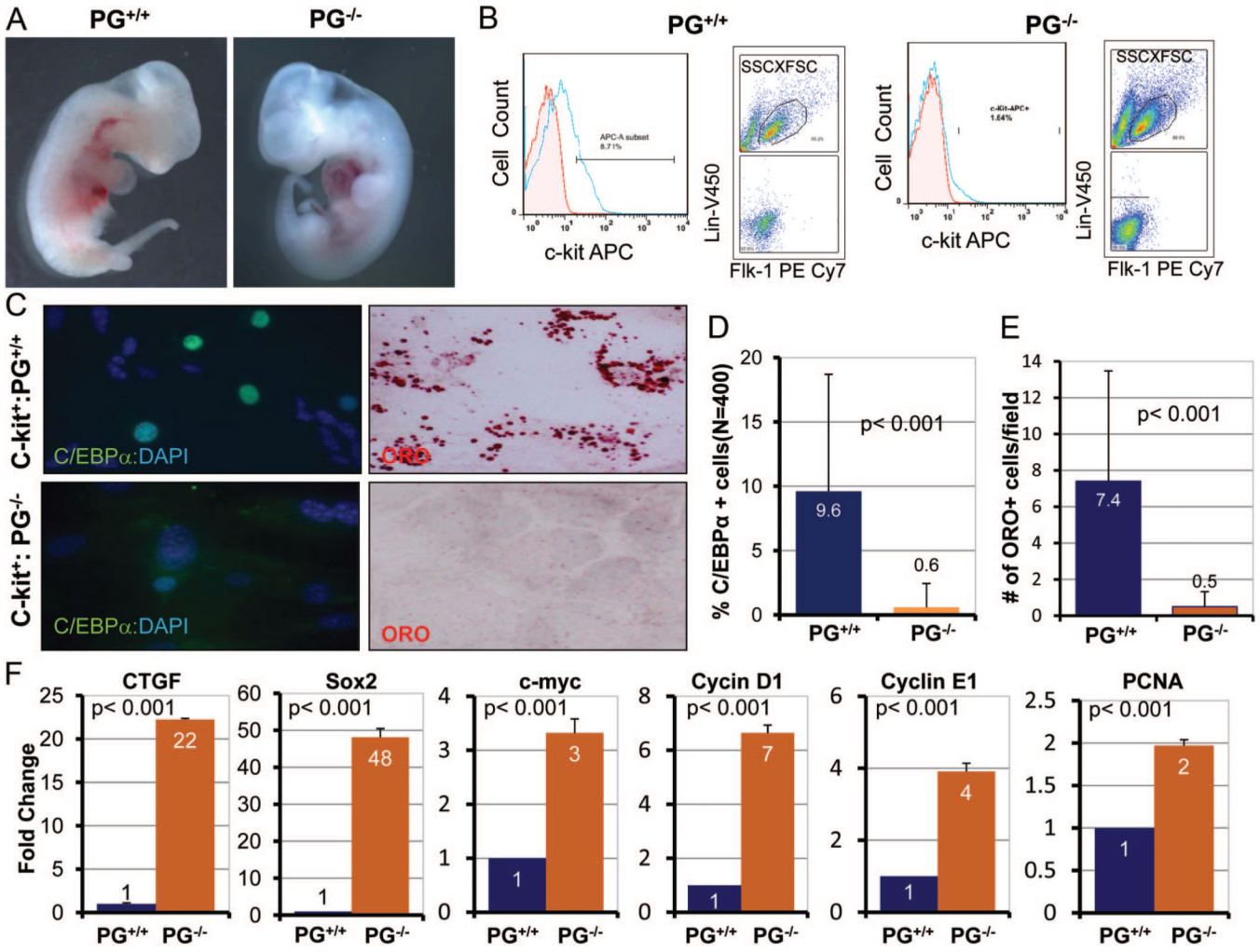

Figure 7. Absence of adipogenesis in c-Kit$^+$ cells isolated from PG$^{-/-}$ embryos

A, Photomicrographs showing PG$^{+/+}$ and PG$^{-/-}$ embryos at E11. **B,** Plots showing the gating steps used to isolate Lin$^-$:Flk-1$^-$:c-Kit$^+$ cells from 11E embryos. A forward and site scatter based gate was initially created. As shown in the back gating plots, a second gate was then drawn to exclude cells expressing markers for hematopoietic lineage (Lin) and Flk-1, an endothelial precursor cell marker. **C,** ORO and C/EBP-α panels illustrate decreased adipogenesis in c-Kit$^+$ CPS isolated from PG$^{-/-}$, as opposed to c-Kit$^+$ cells isolated from PG$^{+/+}$ embryos, despite adipogenic induction. **D** and **E,** Representative quantitative data are shown. **F,** Panels show mRNA levels of selective adipogenic, canonical Wnt signaling, and cell cycle markers by real-time PCR in Lin$^-$:Flk1$^-$:c-Kit$^+$ cells isolated from PG$^{+/+}$ and PG$^{-/-}$ embryos. CTGF, Sox2, c-Myc, and cyclinD1, markers of activation of the canonical Wnt signaling, and mRNA levels of cyclin E1 and PCNA, indicative of cell cycle activation, were increased in PG$^{-/-}$ CPCs.

Table

Echocardiographic Findings in NTG, PG^{WT}, and PG^{TR} Mice

	NTG	PG^{WT}	PG^{TR}	*P* (ANOVA)
N	29	23	25	NA
Sex (males/females)	18/11	12/11	12/13	0.564
Age (months)	9±3	10±4	10±1	0.450
Body weight (g)	31±4	32±5	33±6	0.294
Heart rate (bpm)	573±67	598±76	593±54	0.350
IVST (mm)	0.96±0.09	0.90±0.08*	0.90±0.07*	0.004
PWT (mm)	0.95±0.14	0.90±0.07	0.95±0.09	0.237
LVEDD (mm)	2.80±0.31	3.03±0.26*	3.21±0.44#	<0.001
LVESD (mm)	1.07±0.33	1.16±0.25	1.51±0.55#	<0.001
LV mass (mg)	88±22	90±13	103±23*	0.012
FS (%)	62±9	62±6	54±10#	<0.001
E/A	1.08±0.14	1.24±0.24	1.20±0.31	0.839
Ao V max (m/s)	1.20±0.44	0.98±0.27	1.03±0.14	0.482
ET (ms)	60.36±9.61	49.10±8.57	52.58±8.50	0.002

IVST, interventricular septal thickness; bpm, beats per minutes; PWT, posterior wall thickness; LVEDD, left ventricular end diastolic diameter; LVESD, left ventricular end systolic diameter; LVMass, left ventricular mass; FS, fractional shortening; E/A, ratio of early to late mitral inflow velocities; Ao Vmax, maximum aortic outflow velocity; ET, ejection time; ANOVA, analysis of variance; NA, not applicable.

* $P \leq 0.05$.

$P \leq 0.001$, by Bonferroni pairwise comparison with nontransgenics.